ICAS-88-3.8.1

Some new test results in the adaptive rubber tube test section of the DFVLR Göttingen

A. Heddergott, E. Wedemeyer

Deutsche Forschungs- und Versuchsanstalt für Luft- und Raumfahrt e.V.
Institut für Experimentelle Strömungsmechanik, 3400 Göttingen (FRG)

Abstract

The adaptive rubber tube test section has been in operation now for four years. More test results and experiences have been gained so that the capability of the test section can be compared with other transonic test facilities. While previous tests were mainly performed on thick models producing large blockage effects more recent force- and pressure measurements were made on models of transport airplanes. As a first approach to wall adaptation at supersonic speeds, tests with a cone-cylinder model were performed at a Mach number of 1.2. Most of the test results reported here could be compared with reference data which are considered interference free as they were obtained for small blockage and wing span ratios in wind tunnels with ventilated walls.

1. Introduction

Previous measurements [1, 2, 3, 4, 5, 6] in the adaptive rubber tube test section (DAM) of the DFVLR Göttingen have demonstrated that interference free results can be obtained even at high blockage ratios up to 3.6 %. So far, mainly non-lifting models or models with relatively small lift and large blockage had been investigated (FFA-spindle, ONERA C5 body of revolution, and AGARD-calibration models). In all cases the interferences were dominated by blockage effects, while interferences due to wall induced upwash were only small.

For models having no wings or only slender wings, with a small ratio of wing span to tunnel width, interference free flow can be obtained by merely eliminating wall interferences along the tunnel centreline. This can be done e.g., as shown in Ref. 7, in wind tunnels with only two adaptive walls.

The full 3-D capability of the rubber tube test section can only be demonstrated if the wing span of the model is not a small fraction of the tunnel width. For this reason, measurements have been performed on models having relatively large span and small blockage i.e. models that are typical for transport airplanes.

Previous measurements in the DAM have confirmed a principal limitation of solid wall test sections in the range of transonic Mach numbers. Due to small wavyness of the walls, the flow tends to become choked sooner or later when approaching Ma = 1. It appears that only ventilated walls permit appropriate test conditions in the near sonic range. On the other hand, for supersonic Mach numbers, the main limitation is due to wave reflections on the solid walls, and the question arises, if wave reflections can be alleviated by suitable adaptation of the solid walls. Therefore, additional tests have been made at Ma = 1.2, with a cone-cylinder model.

In the following, a brief description of the rubber tube test section (chapter 2) and the principle of subsonic and supersonic wall adaptation (chapter 3) will be given. In chapter 4 the various models are described and in chapter 5 experimental results are presented.

2. Description of the rubber test section

The fully three-dimensional adaptive wall test section at the DFVLR Göttingen is made of a thick-walled rubber tube, 0.8 m in diameter and 2.4 m long [8]. The test section was installed in the existing High Speed Wind Tunnel (HWG) which is a vacuum storage blow-down tunnel [9]. Fig. 1 shows a schematic drawing of the DFVLR High Speed Tunnel and the new test section. A photograph of the test section is shown in Fig. 2.

A circular cross section was chosen for the rubber tube as it was easy to manufacture and gives a most uniform load distribution on the supporting jacks.

The rubber tube is flanged at one end onto the circular nozzle. The other (free) end extends to the bell-shaped collector. The tube is supported and can be deformed by a set of 64 jacks which are connected to a rigid frame around the test section. The jacks are driven by stepping motors. At each of 8 cross sections 8 jacks are mounted circumferentially with equal angular distances between two adjacent jacks. The hinged connection of the jacks allows for small lateral displacement. Each jack acts via four support points on the rubber wall so that the deforming force is more evenly distributed over the surface. The supports are vulcanized into the rubber wall.

The holes for pressure measurements are located at the 1/4 and 3/4 position between the support points in longitudinal direction and the 1/2 position between the supports in circumferential direction. These have been calculated as positions of minimum error due to wall waviness effects.

Wall pressure and displacement are determined at the 64 positions of the jacks. In addition to the recorded steps of the motors, 64 potentiometers are used for the measurement of the wall displacement.

The measurement of the wall data, the wall adaptation, and the model testing is performed fully automatically [10].

A PSI pressure transducer and acquisition system is used to measure pressure distributions on the test section walls as well as on wind tunnel models.

3. The principle of adaptive walls

3.1 Subsonic wall adaptation

The principle of adaptive walls, which was first described in papers by Ferri & Baronti [12] and Sears [13] is illustrated in Fig. 3.

The method requires the measurement of two independent flow variables at the wall or at another interface surface, for example normal (v) and tangential (u) velocity. An equivalent pair of flow variables are wall pressure (p) and wall displacement (η).

For a given wall contour a fictitious "exterior flow" is defined as a potential flow over and exterior to the wall contour which passes into undisturbed parallel flow at infinity (Fig. 3).

The exterior flow, which can be computed on the basis of potential flow theory, is in general not a physical continuation of the interior flow unless the wall pressure is continuous, i.e., the measured pressure p_i at the inside of the wall agrees with the computed exterior wall pressure p_e at every point on the wall surface. The fluid dynamical problem of wall adaptation is to find a wall contour for which the pressure is continuous across the wall. Usually this problem is solved iteratively. A wall contour is computed which gives an exterior pressure distribution p_e equal to the measured pressure p_i. Then a mean value between the computed and the previous wall contour is taken as the new wall contour. More precisely, a relaxation factor (of about 0.5) is applied to the displacement between computed and previous wall contour. For the displaced wall a new pressure distribution p_i is measured and compared with the new theoretical distribution of p_e. The iteration is continued until the measured interior and the calculated exterior pressure distribution agree within a given error margin.

Under certain conditions the wall adaptation can be achieved with only one iteration step. The one-step method used with the rubber tube test section is based on the assumption that the flow is subsonic near the test section walls and that the wall deflections are sufficiently small so that flow disturbances due to the wall deflections can be described by linearized potential flow theory. Under the above assumption the flow induced by the wall deflections can be superimposed on the flow induced by the model. Then, after wall deflection, the resulting flow variables on the inside of the wall must be equal to the flow variables on the outside. This condition leads to a set of linear equations for the wall deflection. The solution of the linear set of equations gives, with one iteration step, the interference-free wall contour. A detailed description of the algorithm for the calculation of the adapted wall contour is given in [1, 2] and [11].

It is remarkable that the adaptation procedure does not require any model representation. The only input for the computation of the interference free wall contour are the experimental wall data.

In cases where supersonic regions extend up to the test section wall the proposition of linearized flow theory is incorrect and a more elaborate iterative method becomes necessary for the adaptation of the wall.

3.2 Supersonic wall adaptation

As in subsonic testing, wall pressure measurements in the not adapted test section are performed in a preliminary tunnel run. The wall pressure distribution allows to compute the interference free wall contour. If we exclude, for the present, multiple wave reflection at the test section walls, then the measured c_p-values on the straight - not adapted - walls are just twice as large as those, which would exist in unconfined flow. In unconfined flow, the pressure distribution is related - in linear approximation - to the local flow angle Θ by:

$$(1) \qquad \tan\Theta = \frac{\beta}{2} c_p \quad ; \quad \beta = \sqrt{M^2 - 1}$$

Assuming now for c_p one half of the value measured at the walls, $c_p = 1/2(c_p)_{wall}$, Eq. 1 allows us to compute the required wall displacement η in first iteration.

$$(2) \qquad \frac{d\eta}{dx} = \tan\Theta = \frac{\beta}{4}(c_p)_{wall}$$

If multiple reflections occur within the model region,then further iterations are necessary. The walls are properly adapted, when Eq. 1 is satisfied everywhere on the wall surface.

4. Models

All of the models described here have been tested in the rubber tube test section (DAM) and in other wind tunnels so that reference data for comparison are available. The reference wind tunnels, all with perforated test section are:

1. The 1.76 m x 1.75 m S2 MA transonic wind tunnel, ONERA
2. The 1 m x 1 m TWG transonic wind tunnel, DFVLR
3. The 0.89 m x 0.85 m $\sum$ 4 St. Cyr transonic wind tunnel, IAT
4. The 4.88 m x 4.88 m PWT transonic wind tunnel, AEDC

4.1 ONERA M3 model

The model ONERA M3 used for force-measurements is shown in figure 4. Model and support are identical with those tested in the reference test sections (14, 15, 16). In contrast to the AGARD-calibration models, the ONERA M3 model is quite sensitive to Reynolds number effects.

4.2 Swept wing model

The swept wing model [17] used for pressure measurements is shown with the principle dimensions in figure 5. The model is symmetric (profile RAE 101) with respect to the plane z = 0, i.e. the wing has symmetric sections and is symmetrically mounted to

the fuselage. The ratio wing span to tunnel width is for the DAM (rubber tube) 76 % and for the TWG (transonic wind tunnel) 54 %. The model has pressure orifices on the suction side of the wing along the wing sections y/s = 0.215; 0.4; 0.6; 0.925.

The c_p-distributions on the pressure side are obtained by reversal of the angle of incidence.

4.3 Cone-cylinder model

A suitable model for the investigation of shock- and expansion wave cancellation was a cone-cylinder model (Fig. 6). The model which was tested in many other transonic wind tunnels, has a cone angle of 20°, a diameter of 113 mm producing a blockage ratio of 2 %, and a length of ten diameters [18]. To observe wave reflection the model is equiped with 26 static pressure holes along one generating line. The measured pressure distributions have been compared with data from the 16 foot AEDC wind tunnel, which has a very low blockage ratio of 0.008 % and perforated walls, so that the reference data can be considered as interference free [19].

5. Results

An airplane model, ONERA M3, shown in Figure 5 was used for force measurements. The identical model was tested in the ONERA S2 MA tunnel and the DFVLR transonic tunnel TWG. The ratio of wing span to tunnel width was 27 % for the S2 MA and 47 % for the TWG as compared with 67 % for the rubber tube test section DAM.

5.1 Force measurements for the ONERA M3 model

The reference measurements on the ONERA M3 model are limited to three representative Mach numbers and measurements of the drag coefficient versus Mach number at zero incidence. The aerodynamic coefficients $C_L(\alpha)$; $C_L(C_M)$; $C_L(C_{Df})$ and C_{Df} (Ma) are plotted and compared with reference values from other wind tunnels in figures 7 to 10.

The lift coefficient C_L, measured in the DAM, agrees perfectly with the C_L-data from the ONERA S2 MA tunnel which has a six times larger cross section, giving a wing span ratio 2.5 times smaller. For Ma = 0.89 the results of the TWG Göttingen deviate slightly from results of the DAM and ONERA S2 MA. These results show that the perforated test section of the TWG with an open area ratio of 6 % is too open for subsonic tests, a result which is known from previous test experience.

The $C_L(C_M)$ curves (figure 8) also show good agreement with reference data. The forebody drag C_{Df} (figure 9) obtained in DAM systematically deviates from the reference S2 MA-results while the agreement is better with TWG-data. A possible explanation for the surplus value of ΔC_{wf} = 0.002 measured in DAM is, that the surface roughness of the model may have increased during the tests, thus giving rise to an increased skin friction drag.

Figure 10 shows the forebody drag coefficient versus the Mach number. Apparently, the C_{Df} from the $\sum 4$ St. Cyr tunnel deviate even more to higher value than those from the DAM. The diviation of the $\sum 4$ St. Cyr-values is, probably, the result of wind tunnel interference. The drag rise, according to the definition $\partial C_D/\partial Ma = 0.1$, occurs at the same Mach number for the DAM and the S2 MA.

5.2 Pressure distribution measurements on the swept wing model

Figures 11 and 14 show some results of pressure measurements at the wing sections y/s = 0.4 and 0.6 for test Mach numbers of 0.5 and 0.8 and angles of incidence from 0° to 10°. The results are compared with reference data from the TWG Göttingen. The figures also show results from the DAM with not adapted walls for Ma = 0.5; y/s = 0.6 (Figure 11). The large discrepancy between "adapted" and "not adapted" values clearly shows the strong effect of the wall interference. After wall adaptation the agreement with reference data is excellent. The agreement is good for all angles of incidence except for α = 10° at Ma = 0.5 (Figure 12) where deviations are apparent. These deviations are difficult to explain, possibly a different type of flow separation because of different free stream turbulence in the reference tunnel is responsible for the observed discrepancy. The pressure distributions measured for Ma = 0.8 and angles of incidences of $-10 \leq \alpha° 10$ show a good agreement with the reference data (Figure 13).

Figure 14 shows that even at the most outboard wing section y/s = 0.925, which is closest to the wall, good agreement with reference data is obtained.

5.3 Pressure measurements on a cone-cylinder model at supersonic speeds

Adaptation of solid walls to supersonic flow conditions were suggested already by Ganzer et.al. [20] for the octagonal test section at the Technical University Berlin. Similar tests have been performed with the rubber tube test section DAM [21]. For testing at supersonic speeds the upstream part of the rubber tube was used to shape the divergent part of a laval nozzle. The first 3 segments were expanded radially to form the contour of an axisymmetric nozzle for Mach 1.2. (contour no. 2, Figure 15). The Mach number distribution was found to be constant along the remaining length of the empty test section.

A suitable model for the investigation of shock- and expansion wave cancellation was a cone-cylinder with static pressure holes at one circumferential position and spaced along the length of the model.

As in subsonic testing, wall pressure measurements in the non-adapted test section were performed in a preliminary tunnel run. The wall pressure distribution was used to compute the interference free wall contours.

The pressure distribution measured on the model in the straight non-adapted test section is shown on Figure 15. The bow shock is reflected from the wall

and hits the model as shown by the pressure rise at x/d = 5.0. Also, the expansion waves originating at the model shoulder are reflected and produce a pressure drop on the model at x/d = 7.5. If the tube walls are adapted, the interferences are significantly reduced as shown on Figure 16. The calculated wall displacement of Δr = 3,5 mm (.138 inch) at the 6th segment (relative to contour no. 2) produces a convex curvature at the 5th and concave curvature at the 6th segment. The expansion waves generated by the convex curvature at the 5th segment essentially compensate the reflected nose shock, so that only a strongly reduced shock hits the model. Also, the compression waves generated by the concave curvature at the 6th segment compensate the expansion waves originating from the model shoulder.

Obviously, the wide spacing of the jacks precludes finer wall adjustments and still better cancellation of the reflected waves. It should be mentioned that the rubber tube test section was not designed for supersonic testing. Nevertheless, a remarkable reduction of wall interferences could be obtained by the relatively course wall adaptation.

Fig. 17 shows, for comparison, the pressure distribution measured on the same model in the AEDC 16 foot tunnel with 2 % blockage. The tunnel has perforated walls, 6 % open, and holes 60° inclined. The figure shows that even the perforated walls do not yield complete wave absorption.

6. Conclusion

The reference tests presented in this report complete previous tests in so far, as new models of typical transport airplanes have been investigated, where upwash interferences are dominating.

From all experiences so far it can be concluded that any kind of models with any wing span and blockage ratio may be tested interference free in the DAM. The model size is only limited by the requirement that all parts of the model must be located within the "clean" test flow, i.e. outside the boundary layers of the test section walls.

Presently the Mach number range for tests in the adaptive rubber tube is restricted to Mach numbers not larger than about Ma = 0.9. This is because of the limited number of jacks (64) and limited wall thickness of 6 cm. Between the suspension points the wall "hangs down" which leads to blockage at Mach numbers approaching 1. This disadvantage can be alleviated in future designs by increasing the wall thickness and the number of support elements.

First tests at supersonic speeds have shown that compression- and expansion waves, originating from the model, can virtually be absorbed at the tunnel walls by proper wall adaptation. A closer spacing of the jacks would be desirable in order to obtain even better wall adaptation particularly in the region where the bow shock is hitting the wall.

7. References

1. Wedemeyer, E.; Heddergott, A. The rubber tube test section of the DFVLR Göttingen. DFVLR-FB 85-18

2. Wedemeyer, E.; Heddergott, A.; Kuczka, D. Deformable Adaptive Wall Test Section for Three-Dimensional Wind Tunnel Testing. J. Aircraft 22, pp. 1085-1091 (1985)

3. Heddergott, A.; Wedemeyer, E.; Kuczka, D.; Neue adaptive Meßstrecke für den Hochgeschwindigkeitskanal der DFVLR Göttingen. Jahrbuch 1984 der DGLR, Vortrag 84-108b

4. Heddergott, A.; Kuczka, D.; Wedemeyer, E. The adaptive rubber tube test section of the DFVLR Göttingen. ICIASF'85 Record, Stanford University

5. Kuczka, D.; Wedemeyer, E.; Heddergott, A. Measurement of interference free data in an adaptive wind tunnel with flexible walls. DFVLR IB 222 - 84 A 46, 1984

6. Heddergott, A.; Wedemeyer, E. Vergleichsmessungen an zwei Flugzeugmodellen mit großer Spannweite in der adaptiven Meßstrecke DAM. DFVLR-IB 222 - 86 A 27

7. Wedemeyer, E. Wind Tunnel Testing of Three-dimensional Models in Wind Tunnels with Two Adaptive Walls. VKI, TN 147 (1982)

8. Wedemeyer, E.; Heddergott, A. Dehnbare Meßstreckenwände für Windkanäle (Durchführbarkeits-Studie). DFVLR IB 251 80 A 02, 1981

9. Ludwieg, H.; Hottner, T. Hochgeschwindigkeitskanal der Aerodynamischen Versuchsanstalt Göttingen. Z. Flugwiss 7 (1959), No. 10.

10. Bartels, E. Systemanalyse, Pflichtenheft und Systementwurf zur Programmentwicklung des Prozessleitsystems für den Hochgeschwindigkeitskanal Göttingen mit dehnbarer, adaptiver Meßstrecke. DFVLR-AVA IB 562/84/2

11. Müller-Wichards, D.; Gülzow, V. Ein potentialtheoretisches Näherungsverfahren zur Berechnung der Kontur einer adaptiven Meßstrecke. DFVLR IB 262 84 R01

12. Ferri, A.; Baronti, P. A method for transonic wind tunnel corrections. AIAA Journal, Vol. 11, 1973, pp. 64-66.

13. Sears, W.R. Self correcting wind tunnels. The sixteenth Lanchester memorial Lecture, London, May 1973, Calspan Rep. RK-5070-A-2, Juli 1973, The Aeronautical Journal, Vol. 78 (1975), pp. 80-89.

14. Vaucheret, X. Comparison des souffleries transsoniques a l'aide de maquettes etalons homothetiques M1, M2, M3. ONERA-NT-3/537 GY (1971)

15. Vaucheret, X. Comparison des souffleries transsoniques S2 et S3 MA Modane - $\sum$4 St. Cyr - AVA Göttingen - a'aide demaquettes etalons homothetiques. ONERA-NT-4/921 GY (1972)

16. Lorenz-Meyer, W. Vergleichsmessungen an drei geometrisch ähnlichen Eichmodellen eines Transportflugzeugtyps sowie an einem äquivalenten Rotationskörper (Vorschlag: ONERA) im Transsonischen Windkanal der AVA Göttingen. DFVLR-AVA IB 062-72 A 28, 1986.

17. Schneider, W. Druckverteilungsmessungen an Pfeilflügel-Rumpf-Anordnungen bei hohen Unterschall-Machzahlen. DFVLR-AVA 70 A 23 (1970)

18. Lorenz-Meyer, W. Die Strahleigenschaften der Meßstrecke des Transsonsichen Windkanals der AVA. DLR FB 66-19

19. Estabrooks, B.B. Wall interference effects on axisymmetric bodies in transonic wind tunnels with perforated wall test sections. AEDC-TR-59-12

20. Ganzer, U.; Igeta, Y.; Ziemann, J. Design and operation of TU-Berlin wind tunnel with adaptive walls. ICAS Proceedings 1984, Toulouse, Volume 1

21. Heddergott, A.; Stanewsky, E.; Wedemeyer, E. Supersonic wall adaptation in the rubber tube test section of the DFVLR Göttingen. DFVLR-IB 222-87 A 08, 1987. STA Proceedings 1987, Nashville, Tn.

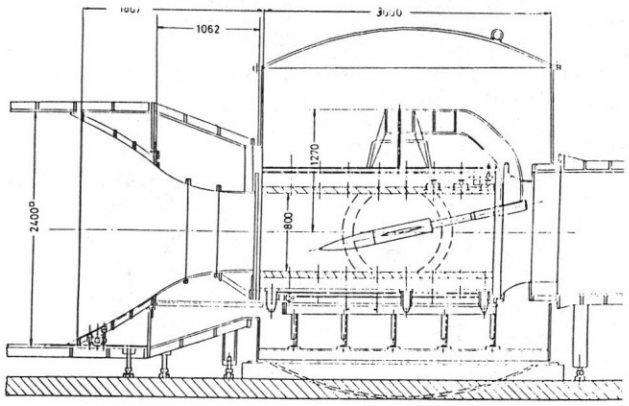

Fig. 1: High speed wind tunnel with deformable adaptive test section

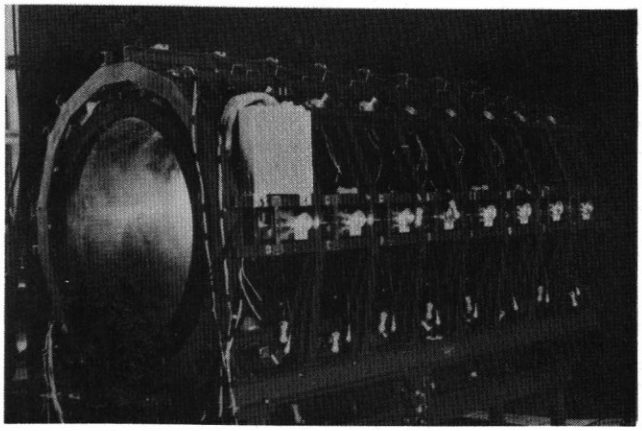

Fig. 2: Photograph of the adaptive rubber tube test section

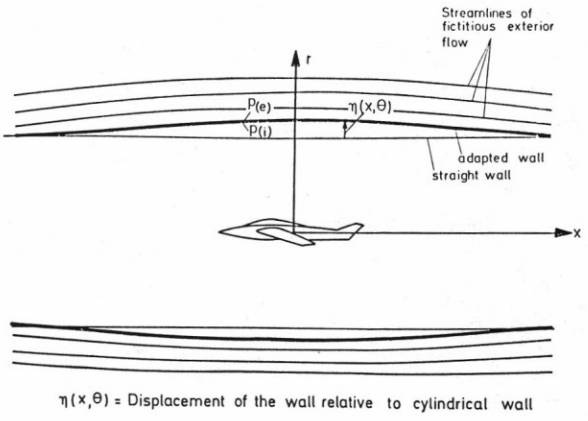

Fig. 3: The principle of adaptive walls

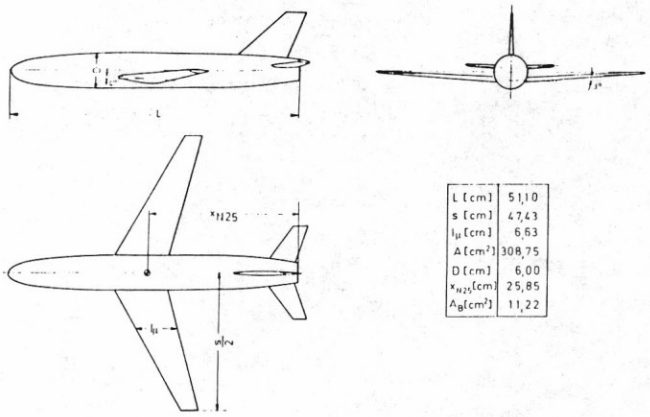

Fig. 4: ONERA M3-Model

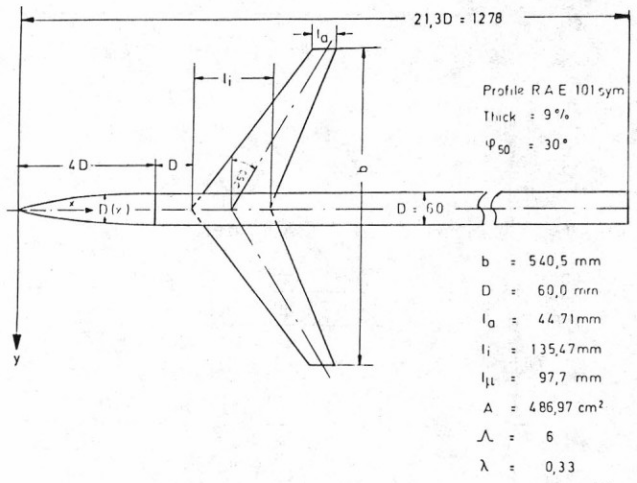

Fig. 5: Swept wing model

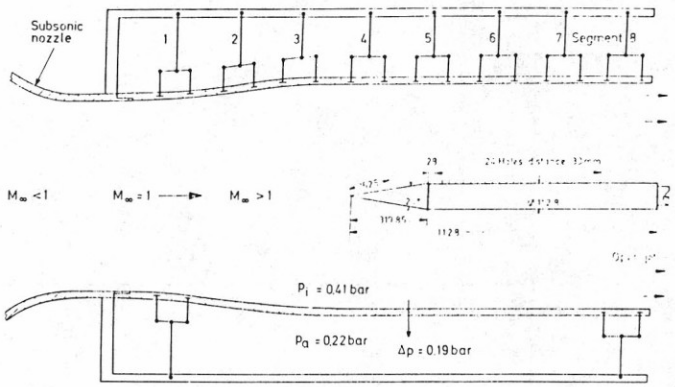

Fig. 6: Rubber tube shaped as Laval nozzle with cone-cylinder model

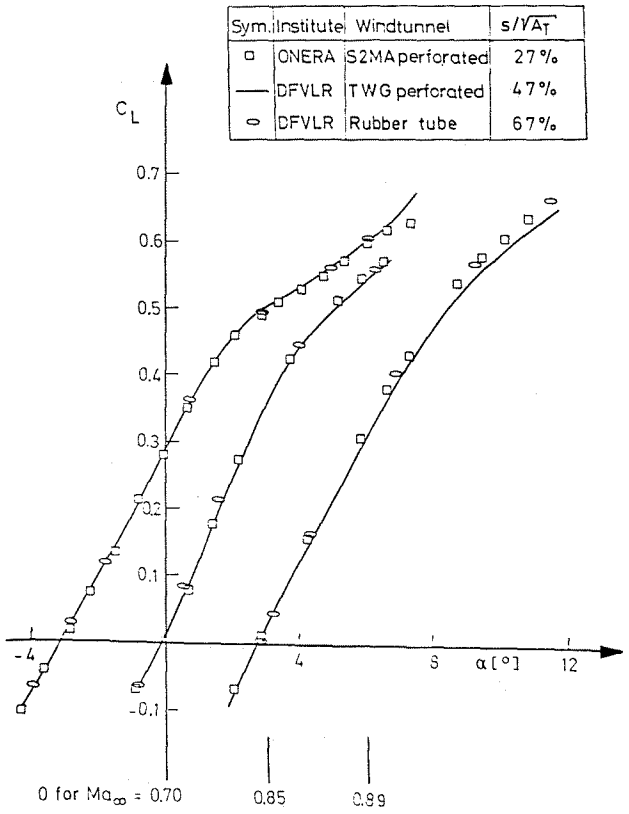

Fig. 7: $C_L(\alpha)$ for ONERA M3 model

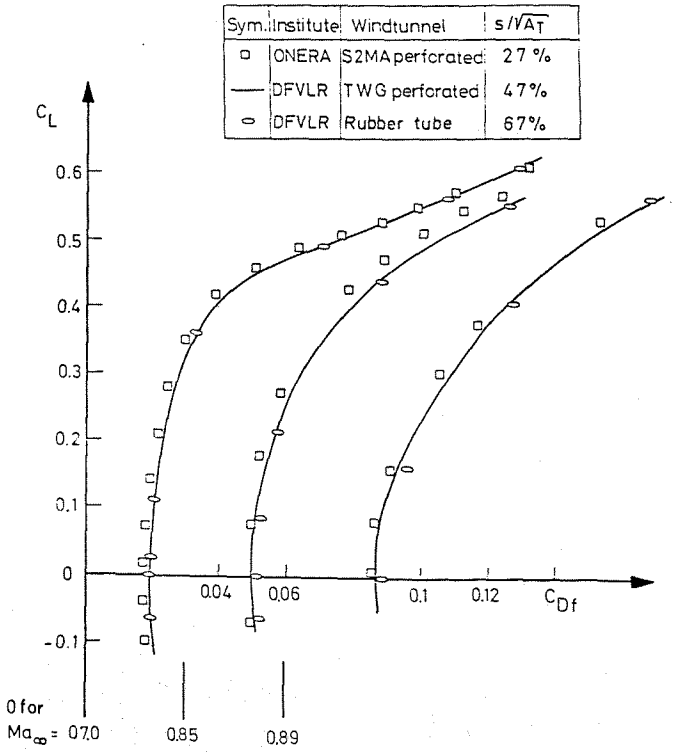

Fig. 9: $C_L(C_{Df})$ for ONERA M3 model

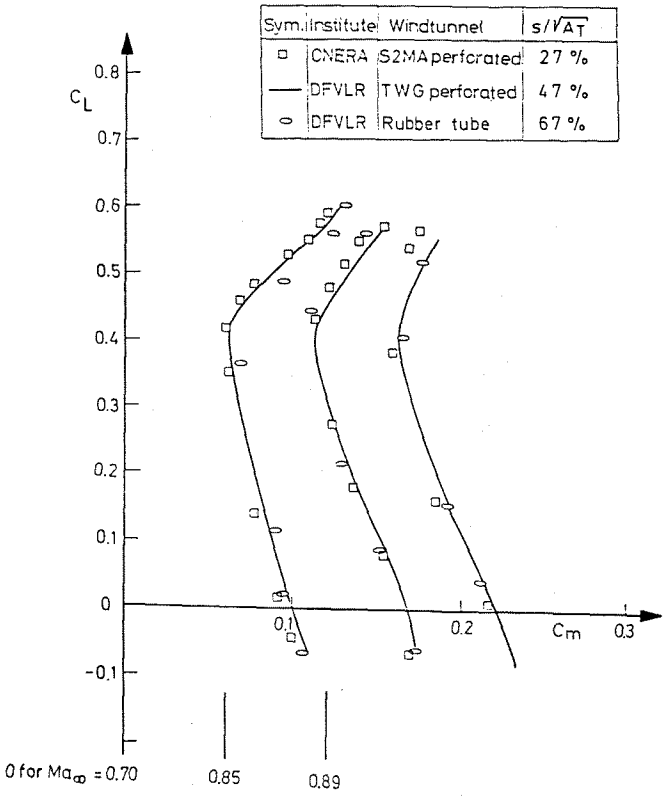

Fig. 8: $C_L(C_M)$ for ONERA M3 model

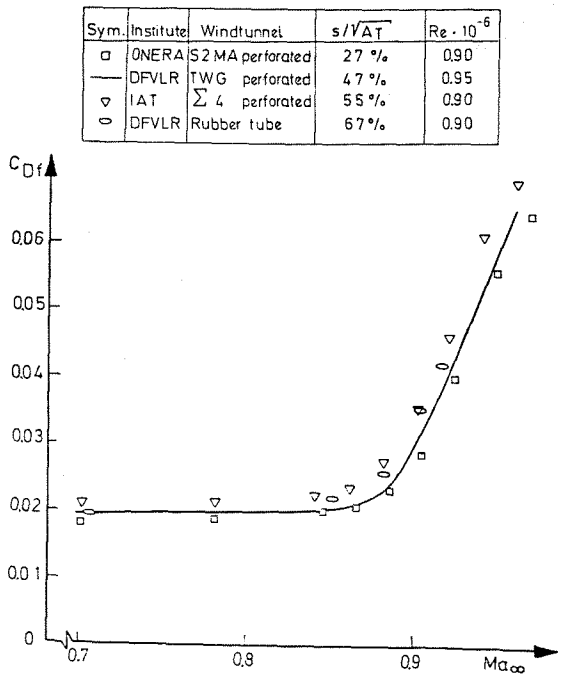

Fig. 10: C_{Df} (Ma) for ONERA M3 model

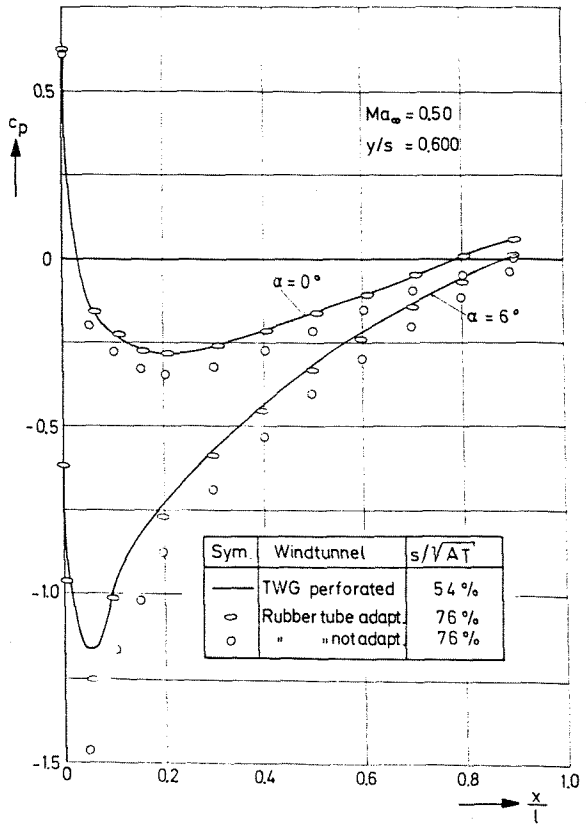

Fig. 11: c_p-distribution for swept wing model

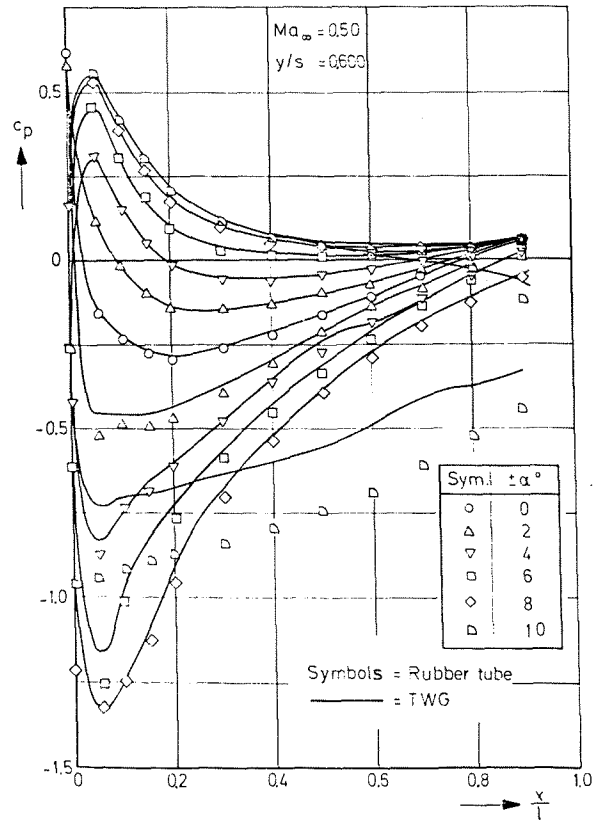

Fig. 12: c_p-distribution for swept wing model

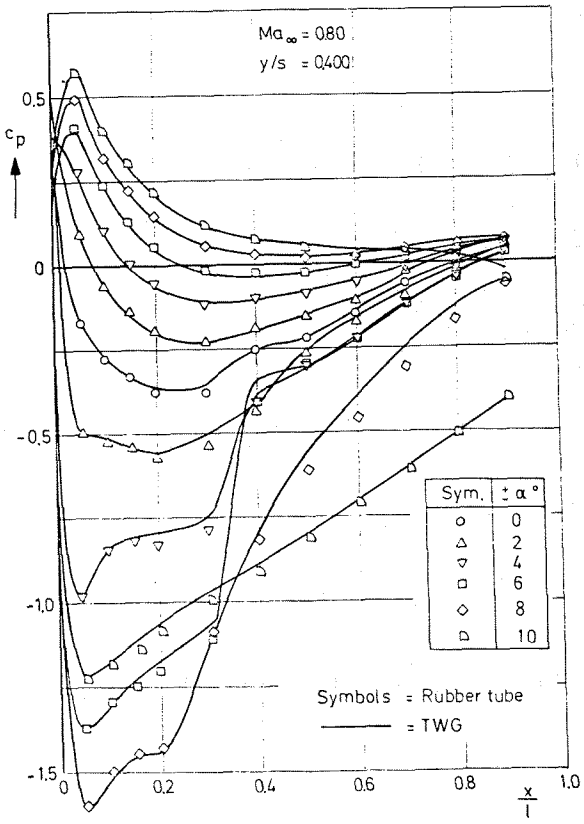

Fig. 13: c_p-distribution for swept wing model

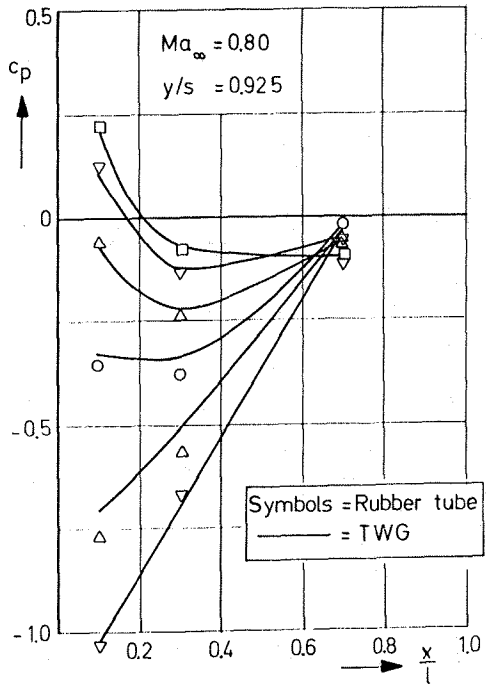

Fig. 14: c_p-distribution for swept wing model

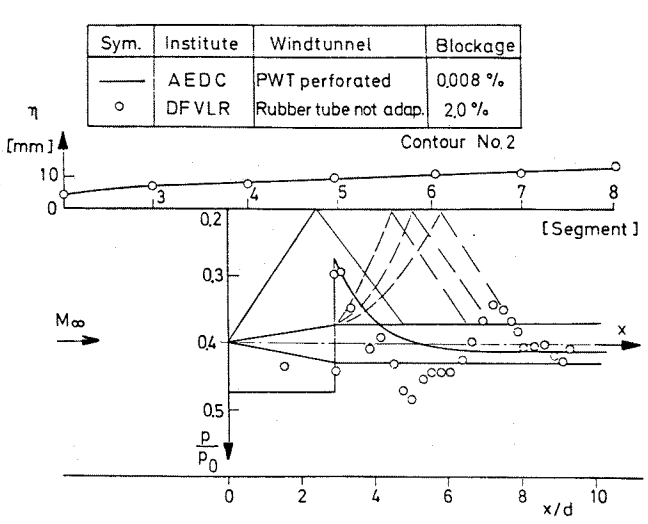

Fig. 15: c_p-distribution on the model before adaptation

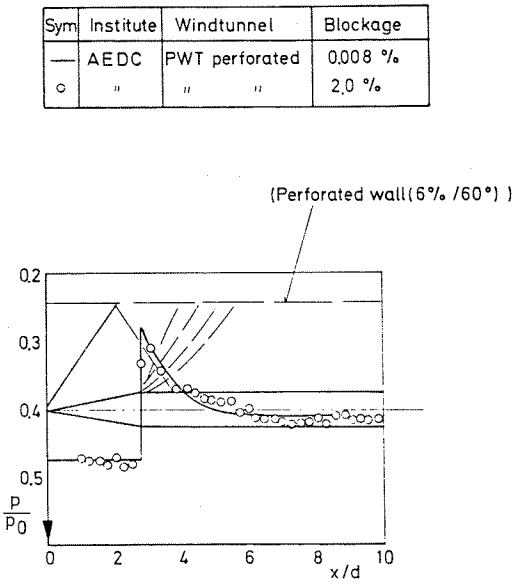

Fig. 17: c_p-distribution on the cone-cylinder model $M_\infty = 1.2$

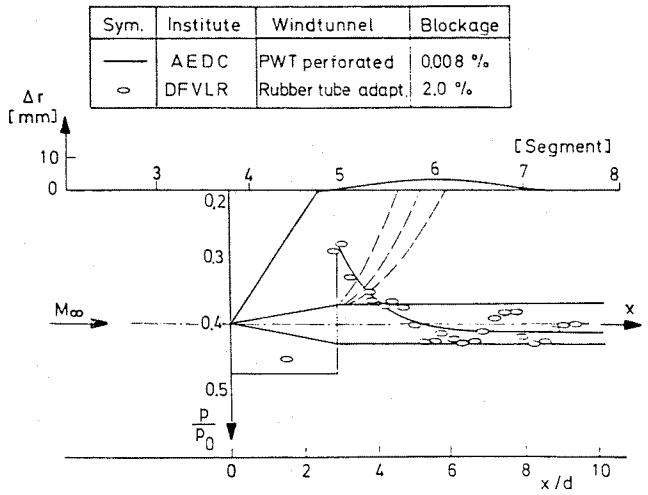

Fig. 16: c_p-distribution on the model after adaptation, Displacement $\Delta r = 3.5$ mm at 6th segment